Journal of Physics: Conference Series

PAPER • **OPEN ACCESS**

A critical insight into the most effective CFD settings to model atmospheric stability in wind energy applications

To cite this article: Riccardo Travaglini *et al* 2024 *J. Phys.: Conf. Ser.* **2767** 092031

Journal of Physics: Conference Series **2767** (2024) 092031 doi:10.1088/1742-6596/2767/9/092031

A critical insight into the most effective CFD settings to model atmospheric stability in wind energy applications

R Travaglini[1], PF Melani[1], F Balduzzi[1], S Orlando[2], V Viti[3], A Bianchini[1]

[1] Department of Industrial Engineering, Università degli Studi di Firenze, Via di Santa Marta 3, 50139, Firenze, Italy.
[2] Ansys Canada, Ltd., 283 Northfield Dr, Waterloo, ON N2J 4G8, Canada
[3] Ansys, Inc., 10 Cavendish Ct, Lebanon, NH 03766, USA

Corresponding author: alessandro.bianchini@unifi.it

Abstract. An accurate reconstruction of the Atmospheric Boundary Layer (ABL) is key for the estimation of energy production and loads in modern wind turbines since, at current rotor heights, the vertical structure of the ABL is heavily influenced by thermal stratification effects. The wind power community usually accounts for these effects by semi-empirical modifications to the neutral ABL profile obtained using linear solvers such as WAsP; this approach, however, may not be suitable for sites with complex terrain, time-dependent thermal effects, or dense canopies. In these applications, methods with higher fidelity, such as Computational Fluid Dynamics (CFD) approaches based on steady or unsteady Reynolds Averaged Navier-Stokes (RANS) equations are needed. While CFD is recognized as providing more accurate results for these realistic cases, its use is still not a common best practice. In the current study, the WindModeller CFD tool by Ansys was employed to assess the effect of various inlet boundary conditions on the predicted wind speed profiles in unstable and stable atmospheric conditions. The test case is a wind farm in North Dakota, USA, characterized by a simple terrain but strong atmospheric stability effects and temperature fluctuations. The comparison of CFD results with experimental measurements and WAsP-CFD simulations reveals a high level of agreement between CFD and experimental data in stable conditions. In the case of unstable conditions, despite the good representation of the wind field, a high sensitivity to inlet boundary conditions is highlighted.

Keywords: Atmospheric Stability, CFD, ABL

1. Introduction and objectives

An accurate reconstruction of the Atmospheric Boundary Layer (ABL) is key for the estimation of energy production and loads in modern wind turbines [1]. At current rotor heights, the vertical structure of the ABL - wind shear and turbulence characteristics - is heavily influenced by thermal stratification effects and atmospheric stability above all. The common practice in industry is to account for these effects by means of semi-empirical modifications to the neutral ABL profile [2] obtained using linear solvers like Wind Atlas Analysis and Application Program (WAsP) [3]. This approach, however, may not be suitable for sites with complex terrain, time-dependent thermal effects, or dense canopies, leading to relevant inaccuracies in wind speed predictions and, in turn, in the actual estimation of the wind resource. To address these challenges, modern high-fidelity simulations based on Computational Fluid Dynamics (CFD) methods, in particular steady (RANS) or unsteady Reynolds Averaged Navier-Stokes

(U-RANS) approaches, have been gaining momentum due to their modeling capabilities and enhanced accuracy. Nevertheless, this field is still evolving and lacks established standards for simulations. Many research efforts have been spent over the years in an attempt to fill this gap. Prior studies [4–6] assessed that the standard approaches included in commercial CFD software, such as k-ε turbulence models and sand-grain rough wall functions, along with the strictly neutrally stable atmosphere, are not sufficiently accurate for modeling the intricate wind flow involved within the ABL. Hargreaves and Wright [7] defined a improved wall function model, consistent with the inflow boundary profiles, to avoid incorrect velocity and turbulence decay along the domain. In particular, they showed that the default law of the wall adopted in the k-ε model to reproduce the rough ground surface needs to be modified in order to correctly maintain the ABL along a lengthy space with no obstacles. Blocken et al. [6] and Parente et al. [8] studied the challenges related to the rough and smooth surfaces treatment. These works focused on modifying the roughness treatment to prevent undesired gradients in mean wind speed and turbulence profiles. Riddle et al. [9], in their study on gas dispersion in a complex urban context, emphasized the importance of using a second-order turbulence closure model, also referred to as Reynolds-Stress Turbulence model. Regarding atmospheric stability, Montavon [10] proposed a formulation of energy conservation and buoyancy term in the vertical velocity equation, in terms of potential temperature. This variable has the advantage of being conserved along the flow trajectories when only adiabatic processes are involved. Moreover, Zilitinkevich et al. [11] introduced a new inlet velocity profile formulation, which implies the existence of the Ekman layer [2]. For this reason, the Coriolis force plays a crucial role in ABL simulations. Despite the significant number of studies on ABL simulation, only a limited number of them have addressed the problem of the most effective boundary conditions (BCs) [12] or a comprehensive description of the setup to obtain the wind flow field in areas with intense stability effects [13]. Most of the studies were focused on the numerical scheme used to solve the flow field, often lacking clear and detailed indications on how to set boundary conditions (BCs) and which assumptions are needed to simulate the ABL structure. The present study aims to fill this gap. Furthermore, it showcases the capabilities of WindModeller (WM), a commercial CFD tool by Ansys, in simulating stability effects on wind flow fields. WM was utilized to simulate the ABL in a wind farm near Wishek, North Dakota (USA), for which experimental data are available. First, a neutral state atmosphere is simulated to define the base numerical framework. Then, simulations for stable and unstable states are conducted on a specific day characterized by strong daily temperature fluctuations.

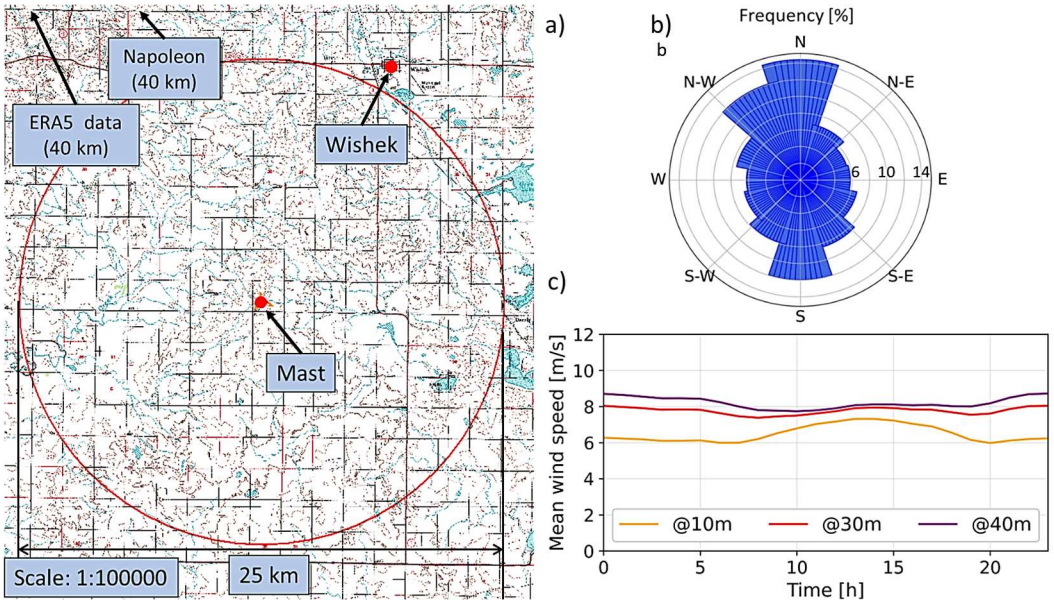

Figure 1. Overview of the Wishek test site: a) topographic map b) wind rose (yearly average) at mast location and height 40m, c) average diurnal wind speed at different heights.

2. Site description

The study was carried out for a wind farm located 14 km from the city of Wishek in North Dakota, USA. This site has a relatively simple terrain (the elevation remains almost unchanged within a diameter of 25 km around the site center) but large temperature fluctuations on both a daily and seasonal basis that significantly impact the measured wind velocity profiles due to atmospheric stability effects (Figure 1c). Measurements used as a benchmark for simulations were collected for a year (01/07/2001-30/06/02) with a one-hour resolution from a single mast at the site center (see Figure 1a) using three anemometers placed at 40 m, 30 m, and 10 m above ground level (a.g.l.), respectively. As shown in Figure 1b, collected wind data indicate North as the prevalent wind direction for the site on an annual basis, conventionally addressed as 0° on the wind rose. This direction is used for the neutral state simulations performed in the present work. Moreover, to highlight the effects of atmospheric stability on wind speed profiles in the same location within a single day, two more simulations were conducted in two specific time frames on July 14th, 2001:

- 2 a.m. reproduces the stable condition, where a reduced turbulent shear production is responsible for high vertical gradients;
- 2 p.m. reproduces the unstable condition, where the ground temperature is higher than the atmospheric one. Thermal convection is responsible for large-scale turbulent movements, which reduce vertical velocity gradients at rotor height.

3. Methodology

3.1. WindModeller

The flow conditions around the site have been simulated with Ansys WM [14], a dedicated wind farm simulation tool that uses the Ansys CFX RANS solver. This tool offers an automated approach for setup and meshing, simplifying the execution of a potentially large number of simulations to predict the wind resource in complex terrains.

3.1.1. Numerical set-up. Numerical simulations were conducted by solving the incompressible unsteady Reynolds-Averaged Navier Stokes (U-RANS) equations, employing the k-ω Shear Stress Transport (SST) two-equation model [15] for turbulence closure. As per standard practice in WM, this model was chosen for its ability to handle variations in the ground surface roughness and flow separation under adverse pressure gradients. In order to include the effects of atmospheric stability, WM uses an approach involving the solution of an additional equation for potential temperature, extensively described in [10]. Furthermore, turbulence production and dissipation due to buoyancy effects are accounted for by including the corresponding additional terms in the k-ω SST model, analogous to the strategy followed in [10] for the k-ε. Finally, Coriolis force effects were accounted for by adding a term to the momentum equation. The role of this last contribution is crucial for the resolution of the Ekman layer and the free atmosphere [2]. Finally, considering the high unsteadiness due to the turbulence introduced by the heat transfer, a time-step size of 10 s was selected.

3.1.2. Computational domain. A cylindrical domain is adopted (see Figure 2 left). The cylinder side face is composed of 24 regions: 12 (red surface) used to prescribe the inflow BC, and the other 12 (blue surface) for the outflow one. The domain outer diameter was selected after a dedicated sensitivity analysis, whose details are reported in [16]. This analysis was performed in *neutral* conditions, i.e., not including thermal effects and limiting the domain height to 4 km.

Table 1. Domain sensitivity.

Dimension	**D1**	**D2**	**D3**	**D4**	**D5**	**D6**
Domain diameter [km]	20	30	40	60	80	100
Domain height [km]	4	4	4	4	4	4

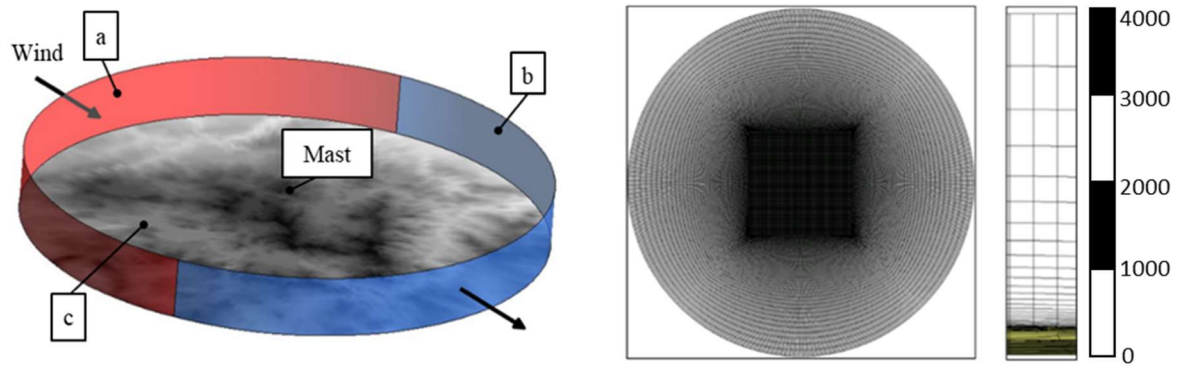

Figure 2. Representation of the computational domain (left) and top and side view of the mesh (right).

Figure 3 (left) shows the results in terms of the wind speed profile sampled at the mast of the domain sensitivity analysis. It can be noted how the smaller domains are not adequate to reproduce the 3-D field in the selected area. The inclusion in the setup of relevant orography and roughness elements, such as the city of Wishek (with domain D2) and Napoleon (with domain D5), led to a progressive convergence of the sampled ABL profile. Based on this observation, domain D5, with a diameter of 80 km, was chosen for the following analyses.

Regarding the meshing procedure, the software starts from a template 5-block topology, which, as shown in Figure 2 (right), is divided into two main areas: a coarser one in the external region and a finer one near the mast (center block). Considering the limited impact on the results observed by enlarging this refined region, its side length was set to 5 km. Through a data-driven script, a structured hexahedral mesh is automatically generated and then projected onto the input ground morphology. To ensure a correct resolution of the ABL, the thickness of the first cell at the ground was set to 5 m, so that the average sand grain roughness *es*, estimated from the average roughness height z_0=0.1m and the von Karman constant *k* (here taken equal to 0.41) via Eq. 1, would fall below its centroid height, as prescribed by [6].

$$es = z_0 * e^{8.14\,k} \tag{1}$$

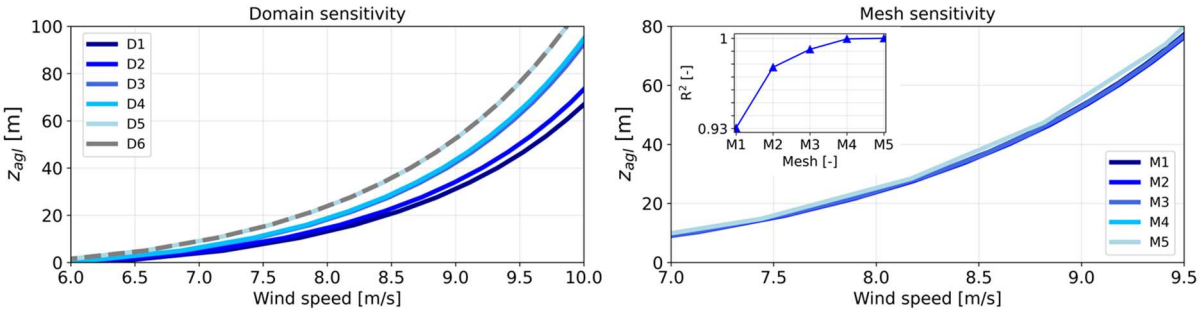

Figure 3. Domain (left) and mesh (right) sensitivity for wind speed at mast location in neutral state atmosphere.

Table 2. Mesh sensitivity.

Dimension	**M1**	**M2**	**M3**	**M4**	**M5**
Spatial resolution (h[m] x v[m])	200 x 160	100 x 80	50 x 40	40 x 30	30 x 20
Center block side length [km]	5	5	5	5	5
# elements [k]	66	364	2070	3731	8619

Moreover, geometric expansion factors of 1.08 and 1.05 were applied to cells in vertical and horizontal directions, respectively. To ensure a mesh-independent solution of the flow field, five different grids were generated from domain D5 with different combinations of horizontal and vertical cell size (see Table 2) and tested in neutral conditions. Figure 3 (right) reports the comparison between the different meshes in terms of the ABL velocity profile at the mast, along with the corresponding coefficient of determination R^2. The latter is defined using as a reference the [16].

Based on the obtained results, mesh M4, with a spatial resolution of 40 m and 30 m in the horizontal and vertical directions, respectively, and a total of 3.73 million hexahedral elements, was selected. Furthermore, even if mesh resolution and domain radius remain unchanged in non-adiabatic cases, to better describe vertical thermal stratification, in the simulation all the layers from the surface one to the free atmosphere [2], the domain height was extended to 10 km.

3.1.3. Boundary conditions. The following boundary conditions were adopted for convective test cases (conventions as in Figure 2):

- **Inlet (a)**: a Dirichlet condition was imposed at the inlet for velocity and turbulence quantities, alongside the application of a Neumann condition for pressure. In detail, the velocity profile was prescribed using the Zilitinkevich formulation [11], i.e., an extended version of the log law in Eq. 2, which requires: 1) the geostrophic wind speed, computed via the geostrophic drag law [17]; 2) the temperature difference (ΔT) between the ground and the mast; 3) the reference wind speed, which is either extrapolated from the mast measurements using the WAsP terrain model or estimated directly from the ERA5 reanalysis data [18] available at the inlet (see Figure 1c); 4) the upstream roughness z_0, calculated as the average between the mean and the most frequent value of roughness within a radius of 10 km from the mast, beyond which the influence of roughness elements becomes negligible [19]. It must be noted that for the inlet wind direction, a deviation of -30° and -40° from North was applied to the stable and unstable cases, respectively, according to the reference data.
- **Outlet (b) and upper domain**: entrainment condition with prescribed atmospheric pressure and temperature.
- **Ground (c)**: No-slip condition. The flux of momentum was determined using wall functions, according to the local roughness value. On the other hand, the ground heat flux was defined by means of the difference ΔT_{ground} between the ground temperature in the real case T_{ground} and the one in adiabatic conditions $T_{ground,ad}$ at the mast location. T_{ground} was taken from ERA5 data at 2 m a.g.l., while $T_{ground,ad}$ was linearly extrapolated at the ground level from mast measurements at 10 m a.g.l., using the dry adiabatic lapse rate for the standard atmosphere. This resulted in ΔT_{ground} values of -3.1 K and 2.2 K for the stable and unstable case, respectively.

3.2. WAsP-CFD

In the present work, simulations with the CFD-based counterpart of the WAsP tool (WAsP-CFD [19]) are carried out to generate an additional reference for the analysis of the obtained results. This methodology exploits the RANS EllypSys3D solver to account for the terrain roughness and orographic profile in the wind field solution. For turbulence closure, the standard k-ε model was selected. To make simulations Reynolds-independent, the effects of Coriolis force and atmospheric stability are neglected. To still account for these effects, WAsP-CFD relies on the WAsP framework, which in turn uses a semi-empirical modification ψ to the standard log law, as in Eq. 2:

$$V(z) = \frac{u_*}{k}\left[\ln\left(\frac{z}{z_0}\right) - \psi\left(\frac{z}{L}\,\frac{kg}{T_0}\,\frac{H_0}{C_P u_*^3}\right)\right] \quad (2)$$

where u* is the friction velocity, k is the Von Kármán constant, T_0 is the ground temperature, and H_0 is the ground heat flux. This correction is applied *a posteriori* to the CFD solution. In the present work, the default value of -40 Wm^{-2} for H_0 is adopted for all analyses. The computational domain has the same configuration of WM (see Figure 2), but with a fixed outer diameter of 30 km and an inner block side

length of 2 km. A multi-block, structured mesh is generated, discretizing the ground surface with a cell size of 20 m, and the ABL with 96 elements along the vertical direction, progressively refining up to 5 cm in the near-surface region.

4. Results

In this section, the results obtained with the different WM set-ups are benchmarked against experimental measurements and WAsP-CFD simulations for the selected neutral (see Section 4.1), stable (see Section 4.2), and unstable (see Section 4.3) cases. It must be noted that, according to the rough wall treatment adopted in the CFX solver [20], the element at the ground in the ABL profiles reported in Figures 4-8 has a wind speed greater than zero as it actually lies above the local roughness height (see Eq. 1).

4.1. Neutral state atmosphere.

Simulations with a neutral atmosphere were carried out to separate the effect of atmospheric stability from that of the terrain. In this case, the inlet velocity profile was prescribed using the standard logarithmic law, considering only the setup with reference wind speed extrapolated with WAsP from the aggregated mast measurements (from here on named *"*: mast inlet"*).

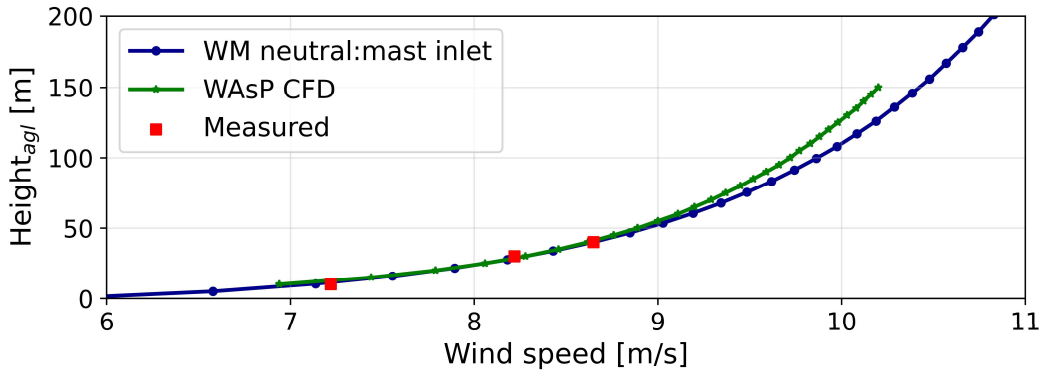

Figure 4. Comparison in terms of wind speed profile at mast location between experiments, WM, and WAsP-CFD for the neutral state atmosphere.

Figure 4 shows the comparison between the WM model outlined in Section 3, WAsP CFD, and experimental measurements in terms of wind speed profile at the mast location. Measured wind data were averaged over a year to filter out the effects of on-site temperature fluctuations. Overall, the agreement between the two models and experiments up to 50 m a.g.l. is good, ensuring the correctness of the adopted strategy for the modelling of the site topology. Above this height, WM and WAsP-CFD start diverging, since the first was run in conventionally neutral configuration, while the second in a slightly stable state, corresponding to the average behavior of the atmosphere.

4.2. Stable state atmosphere.

In Figure 5, the analysis carried out for the *neutral* case (see Section 4.1) is repeated for the *stable* one. In this case, the reference experimental measurements are averaged on an hourly basis (see Section 2), with error bands indicating the corresponding standard deviation, i.e., turbulence level. The same information is not available for numerical simulations due to the selected U-RANS approach, where atmospheric turbulent structures are not resolved.

The WM tool shows a good level of agreement with experimental measurements across all elevations, with minor differences between the mast inlet and the ERA5 inlet configurations, demonstrating its capability to reproduce the stratification conditions commonly occurring when there is a negative heat flux from the ABL to the ground. This is reflected in a flattened wind speed profile if compared with the neutral simulation in the same conditions.

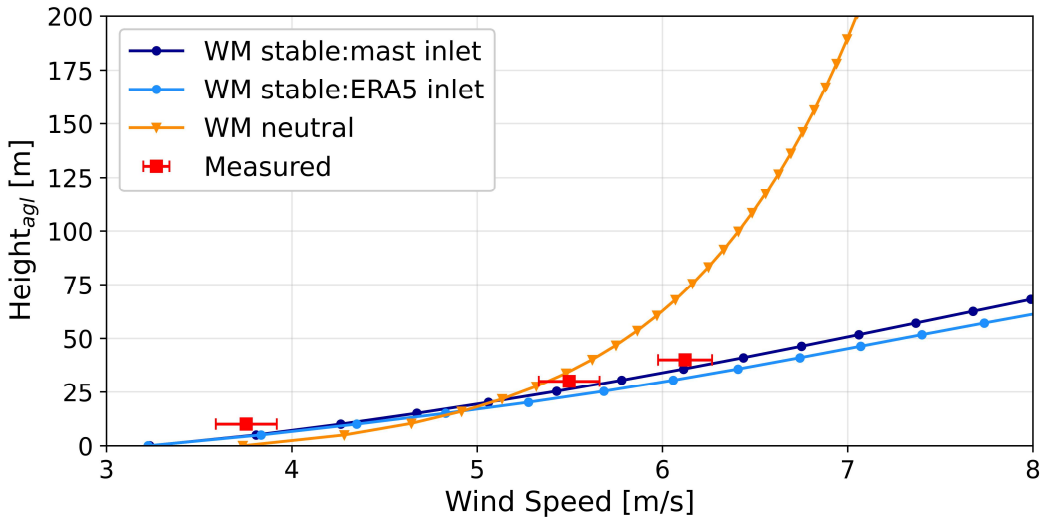

Figure 5. Comparison in terms of ABL profile at mast between experiments, CFD, and WAsP-CFD simulations for the stable state atmosphere.

To gain a deeper understanding of the predicted ABL evolution, Figure 6 shows the development of wind speed vertical profiles throughout the simulation domain in the main wind direction, for six equidistant sampling locations from the inlet to the mast. The terrain altimetric profile is also included to assess the interaction between the ABL and the local orography. Despite the low sensitivity to the setup shown by the results, changes in the wind speed profiles at the inlet affect the flow field.

The different ABL resulting from the *ERA5 inlet* BC leads to a thinner surface layer, consistent with a lower turbulence intensity (I). Consequently, this lower I is responsible for a reduced mixing and a flattened profile, as testified by the results at the mast location. To this end, Figure 6 highlights a surface layer height of 113 m and 125 m for the ERA5 and mast inlet setup (dashed lines), respectively, immediately below the Ekman layer, where wind speed remains almost constant.

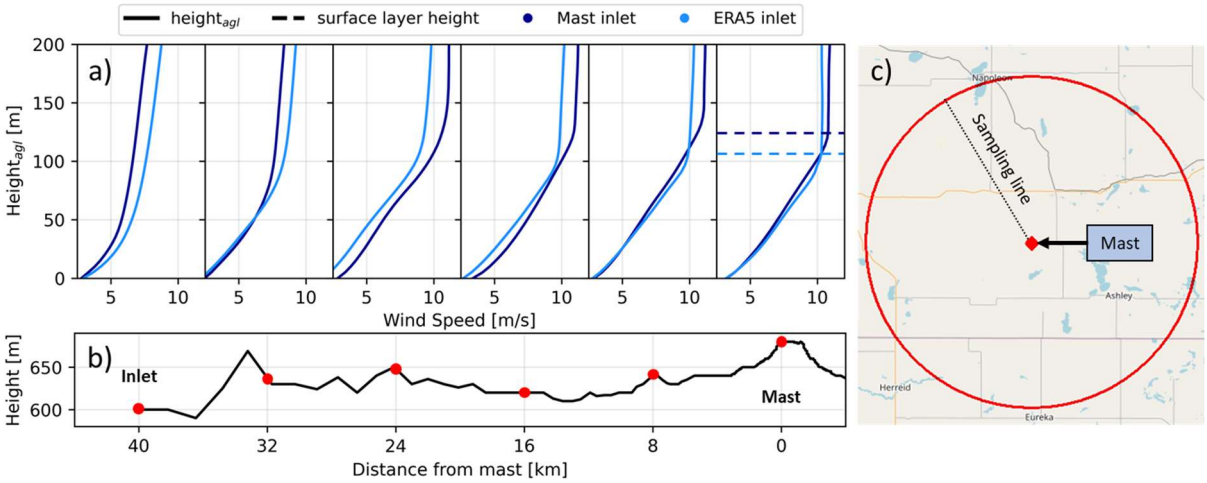

Figure 6. Comparison in terms of wind speed vertical profiles (a) along the main wind direction (c) between the two tested WM setups for the stable case. Terrain elevation profile (b) is also reported.

4.3. Unstable state atmosphere

Figure 7 shows the same plot as Figure 6 for the *unstable* case, assuming 320° as the main wind direction.

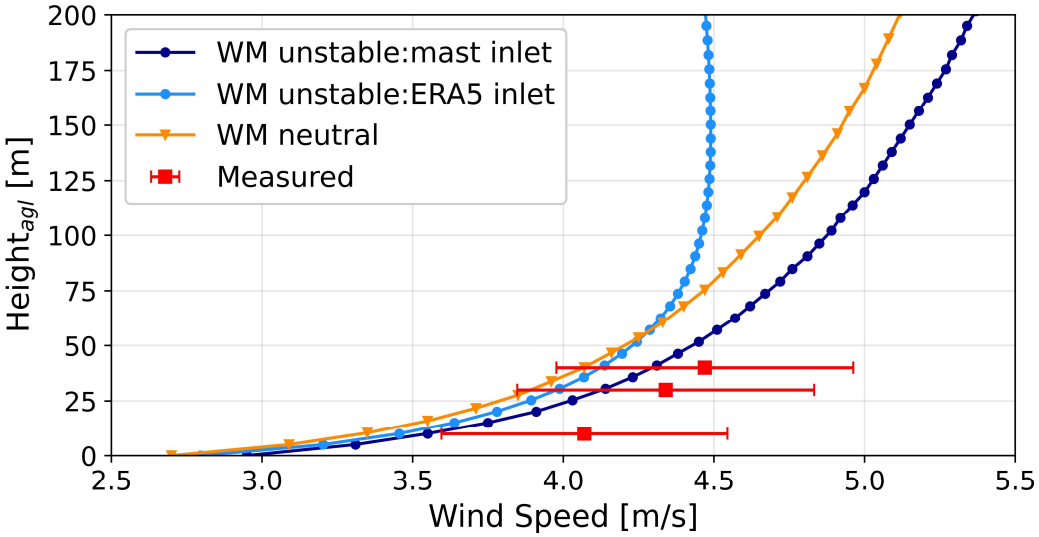

Figure 7. Comparison in terms of ABL profile at mast between experiments and CFD simulations for the unstable state atmosphere.

A larger scattering between the different datasets is observed than in the *stable* case (see Figure 6), highlighting the strong sensitivity of the solution to the adopted numerical set-up and, above all, boundary conditions. The best approximation of the average experimental ABL profile is given by WM with *mast inlet*, with an offset in wind speed of ca. 0.2 m/s between the two datasets. The corresponding velocity distribution is similar, nonetheless, to the one predicted by running the model in *neutral* conditions. The use of ERA5 data to set-up the inlet ABL profile leads, on the other hand, to enhanced mixing in the lower portion of the boundary layer and therefore a steeper velocity profile.

Although this is closer to what would be expected in the unstable case, the wind speed between 10 m and 40 m is largely underestimated. The reason behind the high sensitivity to the inlet boundary conditions observed in Figure 7 can be seen by plotting the ABL evolution throughout the computational domain for the WM: mast inlet and WM: ERA5 inlet configurations, as in Figure 8.

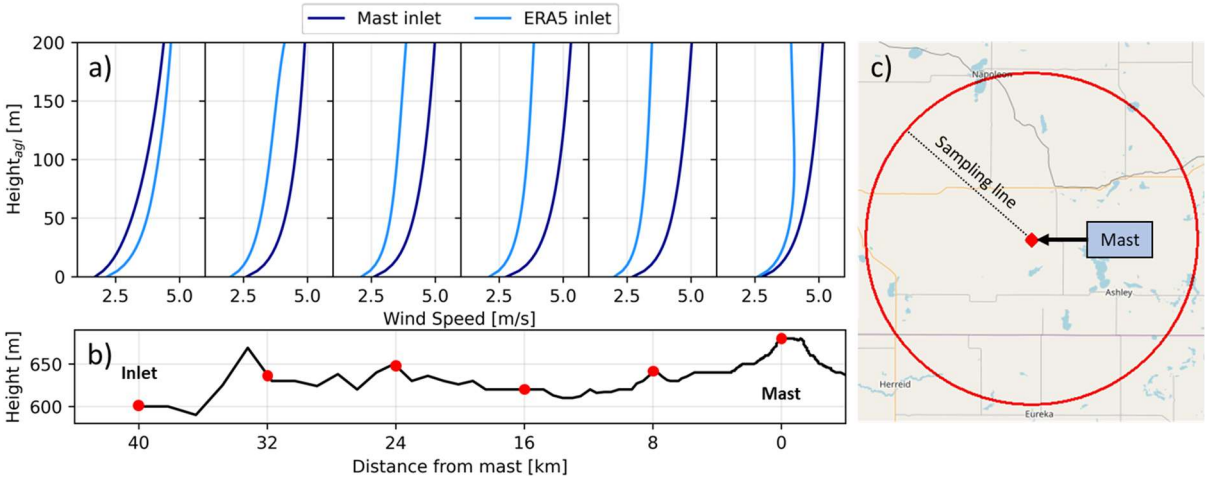

Figure 8. Comparison in terms of wind speed vertical profiles (a) along the main wind direction (c) between the two tested WM setups for the unstable case. Terrain elevation profile (b) is also reported.

At the inlet, no relevant difference in the shape of the imposed ABL profile is observed. As this evolves throughout the domain, the *WM: ERA5 inlet* profile is progressively distorted by the acceleration of the upper part of the surface layer (75 m < height$_{agl}$ < 200 m) with respect to the other ABL regions.

This phenomenon, similar to an inertial oscillation, probably derives from a mismatch between the computed geostrophic wind speed and the velocity at reference height. Additionally, this setup reproduces enhanced stability effects if compared with the mast inlet case, which has a more flattened shape, closer to the neutral profile.

As shown by the cross section of the domain in the prevalent wind direction reported in Figure 9 (right), it is apparent that, in the unstable case, WM reproduces higher turbulence levels up to 450 m. Thermal convection enhances the movement of air parcels, which increases the mixing of adjacent layers and reduces the vertical gradients.

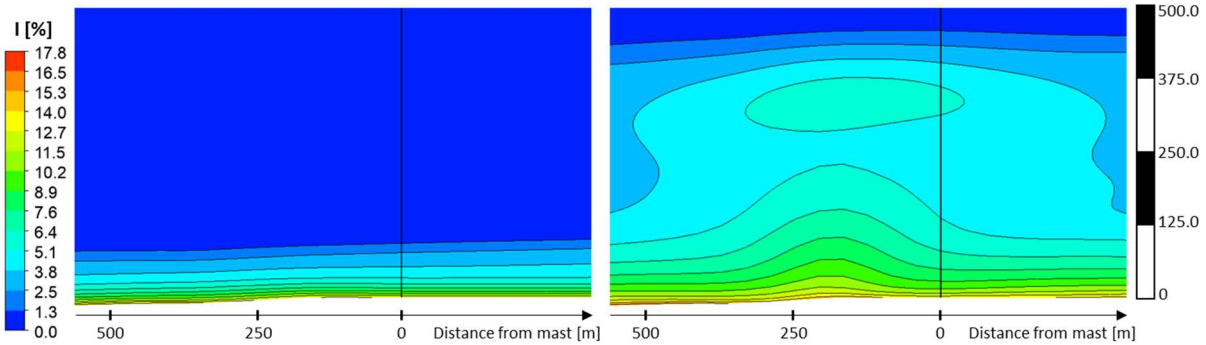

Figure 9. Comparison in terms of turbulence intensity at mast between stable (left) and unstable (right) simulations.

5. Conclusions

The study undertakes an investigation on some of the most effective settings to be used in RANS CFD simulations to accurately reproduce atmospheric stability's influence on wind behavior. The use of a dedicated CFD framework, as employed herein, provided consistent results in both stable and unstable cases. Nevertheless, the dedicated sensitivity analyses showed that, even in sites with non-complex terrains, the accuracy of the solution is strongly affected by the selected set-up, especially in unstable cases where small discrepancies in the prescription of the inlet ABL profile can lead to large oscillations in the solution. Conversely, in stable atmospheric conditions, more accurate results and a lower sensitivity of the solution to the BC are observed. For these reasons, an appropriate specification of BCs is key for the correct simulation of the ABL. Specifically, prescribing the inlet wind speed profile through databases, such as ERA5, or employing extrapolation techniques that consider the morphology of the terrain, can greatly enhance the accuracy of the solution. From this perspective, the outcomes of the study will serve as a useful guideline for future works, where stability effects can be combined with complex terrain morphology.

References

[1] Veers P, Bottasso C L, Manuel L, Naughton J, Pao L, Paquette J, Robertson A, Robinson M, Ananthan S, Barlas T, Bianchini A, Bredmose H, Horcas S G, Keller J, Madsen H A, Manwell J, Moriarty P, Nolet S and Rinker J 2023 Grand challenges in the design, manufacture, and operation of future wind turbine systems *Wind Energy Science* **8** 1071–131

[2] Pérez Albornoz C, Escalante Soberanis M A, Ramírez Rivera V and Rivero M 2022 Review of atmospheric stability estimations for wind power applications *Renewable and Sustainable Energy Reviews* **163** 112505

[3] Troen L and Lundtang Petersen E 1989 *European Wind Atlas* (Roskilde: Risø National Laboratory)

[4] Vermeer L J, Sørensen J N and Crespo A 2003 Wind turbine wake aerodynamics *Progress in Aerospace Sciences* **39** 467–510

[5] Hanjalic K 2005 Will RANS Survive LES? A View of Perspectives *Journal of Fluids Engineering* **127** 831–9

[6] Blocken B, Stathopoulos T and Carmeliet J 2007 CFD simulation of the atmospheric boundary layer: wall function problems *Atmospheric Environment* **41** 238–52
[7] Hargreaves D M and Wright N G 2007 On the use of the k–ε model in commercial CFD software to model the neutral atmospheric boundary layer *Journal of Wind Engineering and Industrial Aerodynamics* **95** 355–69
[8] Parente A, Gorlé C, van Beeck J, and Benocci C 2011 Improved k–ε model and wall function formulation for the RANS simulation of ABL flows *Journal of Wind Engineering and Industrial Aerodynamics* **99** 267–78
[9] Riddle A, Carruthers D, Sharpe A, McHugh C and Stocker J 2004 Comparisons between FLUENT and ADMS for atmospheric dispersion modelling *Atmospheric Environment* **38** 1029–38
[10] Montavon C 1998 *Simulation of atmospheric flows over complex terrain for wind power potential assessment* (Lausanne: EPFL)
[11] Zilitinkevich S, Johansson P-E, Mironov D V, and Baklanov A 1998 A similarity-theory model for wind profile and resistance law in stably stratified planetary boundary layers *Journal of Wind Engineering and Industrial Aerodynamics* **74–76** 209–18
[12] Javier Sanz R et al 2020 The New European Wind Atlas Model Chain *J. Phys.: Conf. Ser.* 1452 012087
[13] Richards P J and Norris S E 2019 Appropriate boundary conditions for computational wind engineering: Still an issue after 25 years *Journal of Wind Engineering and Industrial Aerodynamics* **190** 245–55
[14] Montavon C, Jones I, Staples C, Strachan C, and Gutierrez I 2009 Practical Issues in the Use of CFD for Modelling Wind Farms *European Wind Energy Conference and Exhibition 2009, EWEC 2009* vol 6
[15] Menter F R 1994 Two-equation eddy-viscosity turbulence models for engineering applications *AIAA Journal* **32** 1598–605
[16] Balduzzi F, Bianchini A, Ferrara G and Ferrari L 2016 Dimensionless numbers for the assessment of mesh and timestep requirements in CFD simulations of Darrieus wind turbines *Energy* **97** 246–61
[17] Garratt J R 1994 Review: the atmospheric boundary layer *Earth-Science Reviews* **37** 89–134
[18] Hersbach H, Bell B, Berrisford P, Hirahara S, Horányi A, Muñoz-Sabater J, Nicolas J, Peubey C, Radu R, Schepers D, Simmons A, Soci C, Abdalla S, Abellan X, Balsamo G, Bechtold P, Biavati G, Bidlot J, Bonavita M, Chiara G, Dahlgren P, Dee D, Diamantakis M, Dragani R, Flemming J, Forbes R, Fuentes M, Geer A, Haimberger L, Healy S, Hogan R J, Hólm E, Janisková M, Keeley S, Laloyaux P, Lopez P, Lupu C, Radnoti G, Rosnay P, Rozum I, Vamborg F, Villaume S and Thépaut J 2020 The ERA5 global reanalysis *Q.J.R. Meteorol. Soc.* **146** 1999–2049
[19] Troen I and Hansen B O 2015 Wind resource estimation in complex terrain: Prediction skill of linear and nonlinear micro-scale models
[20] Lechner R and Menter F 2004 Development of a rough wall boundary condition for -based turbulence models Technical Report Ansys / TR-04-04.